J. Fluid Mech. (1985), *vol.* 153, *pp.* 313–337
Printed in Great Britain

Pulsating flow in a pipe

By L. SHEMER, I. WYGNANSKI AND E. KIT
Department of Fluid Mechanics and Heat Transfer, Faculty of Engineering,
Tel-Aviv University, Ramat-Aviv 69978, Israel

(Received 27 April 1982 and in revised form 24 October 1984)

Turbulent and laminar pulsating flows in a straight smooth pipe are compared at identical frequencies and Reynolds numbers. Most measurements were made at a mean Reynolds number of 4000, but the influence of Re was checked for $2900 < Re < 7500$. The period of forcing ranged from 0.5 to 5 s, with corresponding change in the non-dimensional frequency parameter $\alpha = R\sqrt{(\omega/\nu)}$ from 4.5 to 15. The amplitude of the imposed oscillations did not exceed 35% of the mean in order to avoid flow reversal or relaminarization. Velocities at the exit plane of the pipe and pressure drop along the pipe were measured simultaneously; velocity measurements were made with arrays of normal hot wires. The introduction of the periodic surging had no significant effect on the time-averaged quantities, regardless of the flow regime (i.e. in both laminar and turbulent flows). The time-dependent components at the forcing frequency, represented by a radial distribution of amplitudes and phases, are qualitatively different in laminar and turbulent flows. The ensemble-averaged turbulent quantities may also be represented by an amplitude and a phase; however, the non-harmonic content of these intensities increases with increasing amplitude of the imposed oscillations. A normalization procedure is proposed which relates phase-locked turbulent flow parameters in unsteady flow to similar time-averaged quantities. An integral momentum equation in a time-dependent flow requires that a triad of forces (pressure, inertia and shear) will be in equilibrium at any instant of time. All the terms in the force-balance equation were measured independently, providing a good check of data. The analysis of the experimental results suggests that turbulence adjusts rather slowly to the local mean-flow conditions. A simple eddy-viscosity model described by a complex function can account for 'memory' of turbulence and explain the different phase distribution in laminar and turbulent flows.

1. Introduction

The importance of studying time-dependent flows in general, and pulsating pipe flow in particular, is obvious. Most biological flows are pulsating, perhaps because the peristaltic pump is the simplest pump employed by a biological system. Pulsating pipe flows were therefore extensively studied by investigators concerned with medicine or biology (e.g. Caro *et al.* 1978; Hussain 1977). Non-steady flows occur also in many engineering applications, for example: the discharge of any piston pump is pulsating, the flow in an intake or exhaust manifold of an internal combustion engine is pulsating, the flow in hydraulic or pneumatic lines and control systems often pulsates.

The periodic nature of this type of turbulent flow suggests the decomposition of any flow variable $g(x,t)$ into 3 components (Hussain & Reynolds 1970)

$$g(x,t) = \bar{g}(x) + \langle g(x,\phi)\rangle + g'(x,t), \tag{1}$$

where $\bar{g}(x)$ is the temporally averaged value of the variable $g(x,t)$ at point x and $\langle g(x,\phi)\rangle$ is the contribution of the periodic part at a phase angle ϕ at the same point x. A distinction is sometimes made between 'pulsating' and 'oscillating' flows; the former term is used whenever the oscillations are superimposed on a non-vanishing steady velocity, while 'oscillating' flow refers to $\bar{g}(x) = 0$. The phase-dependent part of the flow, $\langle g\rangle$, is referred to as the oscillating part.

Assuming that the flow is not only periodic, but also harmonic, the periodic component may be represented by the real part of the exponential

$$\langle g(x,\phi)\rangle = \mathrm{Re}\{[\langle g(x)\rangle]\exp(\mathrm{i}(\omega t - \phi_g))\}, \tag{2}$$

where $[\langle g(x)\rangle]$ is the amplitude of pulsations while $\phi_g(x)$ is a phase lag angle. All phase angles mentioned in this work refer to the phase of the pressure drop. Whenever a periodic motion is not simply harmonic the time-dependent variable can always be expanded in Fourier series, and the right-hand side of (2) will become the leading term in the expansion.

The first solution for the velocity distribution in the fully developed oscillating pipe flow was obtained by Sexl (1930). Womersley (1955), Uchida (1956) and others solved the problem again and calculated the phase and amplitude relationship among the pressure gradient, the mean bulk velocity and the shear stress. Since Uchida's solution is presented in the most convenient form, it will serve as the main reference.

Denison (1970) and Denison, Stevenson & Fox (1971) reported on measurements made in pulsating laminar flow with directionally sensitive laser velocimeter. The experimental results obtained at a mean Reynolds number of about 1000 and frequency parameter $\alpha = R(\omega/\nu)^{\frac{1}{2}}$ varying from 4 to 6 agreed with the theory of fully developed flow. Kirmse (1979) used a laser-Doppler anemometer to measure pulsating turbulent pipe flow in water at high frequencies ($55 < \alpha < 137$). The phase shift between pressure and velocity at all radial positions and at all frequencies was found to be 90°. An eddy-viscosity model predicted reasonably well the time-dependent velocities in this flow. Ramaprian & Tu (1980) observed that at mean $Re = 2200$ the phase of velocity pulsations in the central region of the pipe lagged behind the pulsations near the wall. Poor angular resolution in their experiments prevented them from getting quantitative information on phase angles. The velocity profiles, measured in laminar pulsating flow, were in good agreement with the theoretical results of Uchida, and it was concluded that the imposed oscillations have no effect on the time-averaged properties of the flow. In the later work, Tu & Ramaprian (1983) performed measurements in turbulent pulsating pipe flow at $Re = 50000$. They concluded that at low frequencies of pulsations (compared to the bursting frequency) there is no significant influence of pulsations on time-mean $Re = 5.7 \times 10^4$ for a wide range of frequencies. The time-averaged flow was not affected by the imposed oscillations. Three flow patterns – quasi-steady, intermediate, and inertia dominated – were distinguished in the oscillatory component of the flow. The transition from one pattern to another was found to be dependent on the frequency parameter α and on the average Reynolds number. The data-acquisition method precluded the possibility of obtaining ensemble-averaged results and therefore only short-time-averaged data was analysed.

Each of the above investigations was carried out in either laminar- or turbulent-flow regimes. Since our eventual goal is to understand transition from laminar to turbulent flow it was advisable to study a case in which all controllable parameters (e.g. α, Re) remain invariant when the flow is switched from a fully developed laminar to a fully developed turbulent regime. This decision restricts the choice of some experimental parameters, in particular Re.

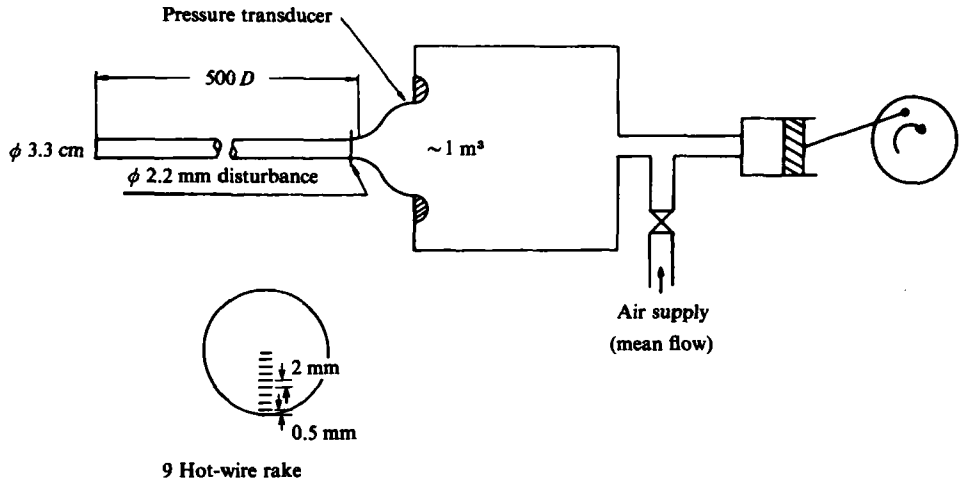

FIGURE 1. The experimental facility.

The most severe limitation on the choice of Re stems from the fact that for a fully developed laminar pipe flow the parameter $(x/D)/Re \geqslant 0.1$ (Wygnanski & Champagne 1973). Thus for a pipe of length 500 diameters the Reynolds number should not exceed 5000. On the other hand, detailed measurements in the wall region in the turbulent pulsating flow can be only made at low Re and, therefore, most of the measurements in this investigation were carried out at $Re = 4000$. Laufer (1954) showed that most of the differences between fully developed pipe flow at $Re = 5 \times 10^4$ and $Re = 5 \times 10^5$ occurred near the wall (i.e. at $r/R \geqslant 0.8$). Lowering the Re by an additional order of magnitude (i.e. to $Re = 4.2 \times 10^3$ (Wygnanski & Champagne 1973) and comparing the data with measurements made at $Re = 5 \times 10^4$ did not indicate a larger difference than that already observed by Laufer between $Re = 5 \times 10^4$ and $Re = 5 \times 10^5$. Even at the lowest Re considered the characteristic frequency of turbulence was at least one order of magnitude higher than the frequency of the imposed oscillations.

The present investigation examines the interaction between the imposed oscillations and the random turbulent motion. The relaxation of turbulence as it passes through the forcing cycle was considered for the purpose of theoretical modelling. The experiments reported were carried out in air at $2900 \leqslant Re \leqslant 7500$ and at dimensionless frequency $4.5 \leqslant \alpha \leqslant 15$. At these frequencies compressibility effects in the pipe can generally be neglected although the response of the entire system to changes in volume and ensuing pressure oscillations were considered (Shemer 1981). Neither flow reversal nor turbulent–laminar transition occurred in any of the experiments reported thus far. Both phenomena can happen whenever the amplitude of the imposed oscillations is large.

2. A general description of the experimental procedure

A straight, smooth aluminium pipe 33 mm in diameter and 500 diameters long was used. The facility, shown schematically in figure 1, was originally used by Wygnanski & Champagne (1973), and described in detail in their paper. As a result of careful alignment and smooth inlet, laminar flow could be retained at Reynolds numbers exceeding 2×10^4 without the addition of screens in the settling chamber. The mean flow was supplied by a high-pressure source (6 atmospheres) controlled by a precise

pressure regulator which ensured that the flow rate was independent of the superimposed pulsations and the flow regime (i.e. whether the flow was laminar or turbulent).

Pressure oscillations were introduced by a valveless piston pump, connected to the settling chamber (see figure 1). The piston diameter was 90 mm, and its displacement could be changed from 5 to 75 mm in 17 discrete steps. The harmonic distortion of the pressure oscillations, defined as the ratio of the power spectrum coefficient at the forcing frequency to the sum of the coefficients at all frequencies in the spectrum, was generally higher than 99%. The pump was driven by 1.5 h.p. variable-speed motor, permitting a change in the period of pulsations between 0.5 and 5 s. The repeatability of the period was better than 0.3%.

Velocity measurements were made with a rake of 9 hot wires, distributed evenly in the radial direction at distances equivalent to $r/R = 0.12$ between neighbouring wires; thus by locating the first wire on the centreline of the pipe the 9th wire was located at a distance 0.5 mm from the wall (i.e. at $r/R = 0.97$). All velocity measurements were taken at the exit plane of the pipe. A 10 channel constant-temperature hot-wire anemometer and 10 channel amplifier were used in the experiment. The output of the amplifier was connected via an analog-to-digital converter to a PDP 11/60 minicomputer for further processing.

The hot wires were calibrated in a wind tunnel, which provided a stable reference velocity between 30 cm/s and 15 m/s. Although flow reversal was avoided, very low velocities occurred in the pipe as a result of the superimposed pulsations. It was thus necessary to calibrate the wires at the lowest velocities anticipated in the experiment. Since a Pitot tube is not an accurate instrument for measuring air velocities below 1.5 m/sec, the frequency of vortices shed by a circular cylinder was used for calibration (Shemer 1981). The calibration of hot wires was done digitally; the detailed description of the calibration procedure may be found in the thesis of Oster (1980) and in Oster & Wygnanski (1982).

A pressure transducer, dynamically responding to 1000 Hz, recorded the pressure at the inlet. The instantaneous gauge pressure divided by the length of the pipe yielded the instantaneous pressure gradient in this experiment. The assumption that the pressure drops linearly was checked experimentally and was shown to be valid. The steady response of the transducer was calibrated against a Fuess micromanometer. The output voltages of the anemometers and the transducer were amplified to match the full range of the 12 bit analog-to-digital converter. The velocity and pressure signals were sampled at a predetermined frequency, and converted into 16-bit words arranged in buffers.

The period of pulsations was determined by the computer at the initiation of each measurement with the help of the optical switch. A cylinder, 1.5 mm in diameter, connected to a flywheel passed at each revolution through a narrow gap of the optical switch, causing a change in the output current, which operated a TTL Schmidt trigger. The trigger signal served as an input to the A/D converter and was sampled at a predetermined rate, controlled by a 1 MHz clock. The period was derived from the number of sampled points between two subsequent trigger pulses, and the result was averaged over 10 cycles.

With the period of pulsations known, the sampling frequency was fixed in such a way that either 1024, 2048 or 4096 points were sampled per channel per period in order to facilitate the processing of data using a Fast Fourier Transform (FFT). The data was acquired continuously by dividing the required memory into two buffers; thus, while one buffer accepted the information sampled, the content of the other buffer was recorded on a magnetic tape. The output of the optical switch was

connected to an additional input channel and provided the required phase information. A total of 11 data channels were thus sampled: 9 channels containing velocity information, 1 pressure and 1 phase information. At present, this method is limited to a maximum sampling rate of 1800 data points per channel per second. This frequency was quite adequate in the range of Re considered. The 'raw' signals recorded on tape were processed at a later stage.

A typical record exceeded 8 periods of pulsations. In laminar flow 7 such records were usually acquired, providing 56 periods containing 1024 sampled points per period. In turbulent flow, the number of records was usually 30, giving 240 periods with the number of points ranging from 1024 to 4096, depending on the duration of the period.

The undisturbed flow was laminar at all Reynolds numbers and frequencies considered. Turbulence was triggered artificially by a protuberance (a cylinder 2.2 mm in diameter) which was inserted diametrically into the pipe 20 diameters downstream of the entrance. The disturbance tripped the flow which became fully turbulent at all Reynolds numbers exceeding 2700. When the cylinder was removed the flow reverted to its laminar state; thus, this simple procedure enabled measurements in laminar or turbulent flows while keeping all other controllable parameters constant.

3. Experimental results

3.1. *Mean flow: steady vs. pulsating velocities and pressure*

The time-averaged parabolic velocity profile in laminar flow was unaffected by the imposed pulsations. Three turbulent velocity profiles, one measured in steady flow, and the other two measured in pulsating flow at identical $Re = 4000$ and period $T = 1.34\ s$ ($\alpha = 8.9$), are compared in figure 2. The relative amplitude of the forced oscillations are 0%, 20% and 35%. No significant difference can be observed between steady and pulsating time-averaged velocity profiles, provided the relative amplitude does not exceed 20%. While independence of mean velocity profile on the imposed oscillations in fully developed laminar flow results from the linearity of the Navier–Stokes equations, in turbulent flow it indicates that the time-averaged Reynolds stresses are also insensitive to forcing. This result is in agreement with the conclusions of most investigators of the pulsating pipe flow. Tu and Ramaprian (1983) obtained, however, different results at $Re = 50000$, in particular at high-frequency oscillations.

The friction coefficient λ, calculated from the Darcy's formula,

$$\frac{\overline{\Delta p}}{\rho} = \lambda \frac{L}{D} \frac{\overline{U}^2}{2},$$

did not show any difference between steady and pulsating flow in either laminar or turbulent regimes. The measured friction coefficient in laminar flow did not differ notably from the value of $64/Re$. In turbulent flow the value of λ was in good agreement with the values quoted in the literature for smooth pipes (see Schlichting 1975).

3.2. *Phase-averaged velocities: laminar vs. turbulent flow*

Phase-averaged data in either laminar- or turbulent-flow regimes provides the first two terms in the decomposition of (1). One may check whether the velocity oscillations are harmonic by expanding the ensemble-averaged signals in Fourier series. The 'power' spectra of these series were calculated, and the ratio of the two

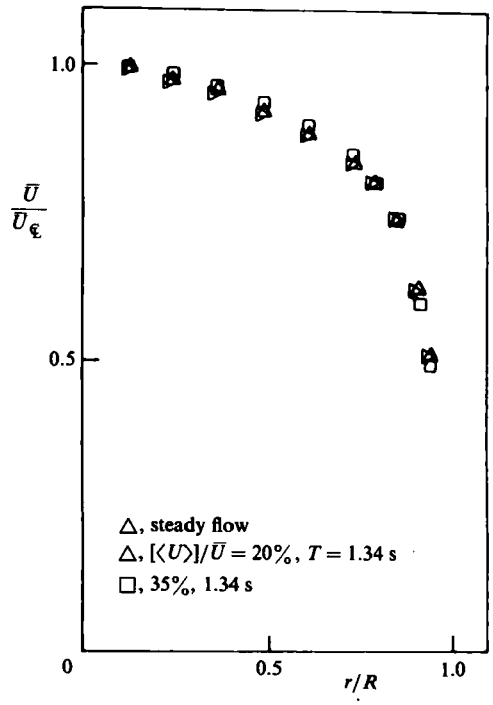

FIGURE 2. Mean turbulent velocity profiles measured at $Re = 4000$.

coefficients corresponding to the fundamental frequency ω_0 and its first harmonic was determined. For moderate amplitudes of velocity oscillations employed in the present investigation, this ratio was less than 3%, thus providing the justification for the harmonic assumption.

The harmonic character of the pulsations enables one to represent the phase-averaged velocity by an exponential form, (2), and alleviates the necessity of describing the temporal and spatial changes in velocity by plotting a large number of velocity profiles. Two functions can fully describe the oscillating component of velocity at the imposed frequency: (i) the amplitude distribution $[\langle u(r)\rangle]$; and (ii) the phase angle $\phi_u(r)$ relative to the phase of the pressure oscillations. In order to obtain these functions, the phase-averaged velocity was Fourier transformed. The coefficients corresponding to the oscillations at the forcing frequency $1/T$ were then used to find the amplitude function $[\langle u(r)\rangle]$ and the initial phase angle $\phi_{u0}(r)$. From the initial phase of the velocity oscillations the initial phase of the pressure oscillations was subtracted, giving phase angles $\phi_u(r)$ relative to pressure.

The dependencies of the measured amplitudes of the cross-sectionally averaged bulk velocity on the imposed pressure oscillations for two frequencies are shown in figure 3. The response of the velocity amplitude to the imposed forcing is hardly affected by the flow régime. The amplitude of the bulk velocity is proportional to the pressure, and within the experimental scatter there is no difference in the slopes between laminar- and turbulent-flow régimes, at least for $T = 2.42$ s ($\alpha = 6.6$). At higher frequency ($\alpha = 8.9$, $T = 1.34$ s) a nonlinearity is noticed when the flow is turbulent, the bulk velocity amplitudes are somewhat higher in turbulent than in the corresponding laminar flow. For a given amplitude of pressure oscillations, the amplitude of the bulk velocity oscillations $[\langle U\rangle]$ depends strongly on frequency. If

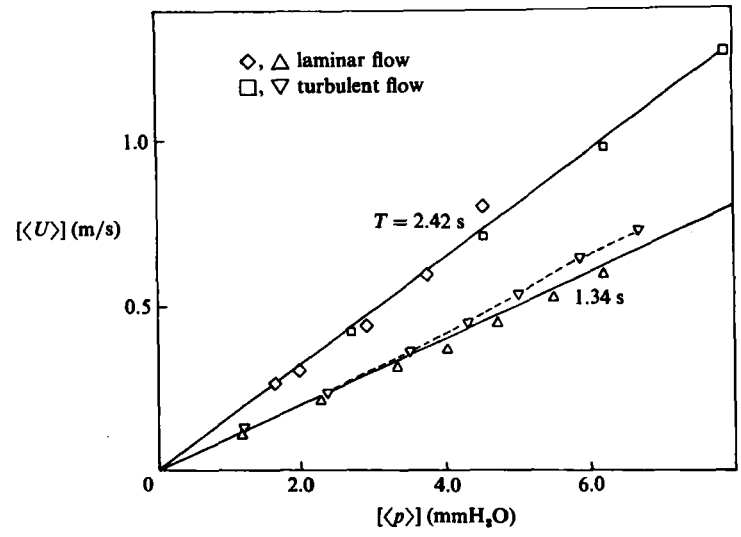

FIGURE 3. The dependence of the amplitude of the bulk velocity on the amplitude of forcing in laminar and turbulent flows at $Re = 4000$.

$\overline{U}$ is the steady part of the bulk velocity ($\overline{U} = \overline{Q}/\pi R^2$, where $\overline{Q}$ is the mean flow rate) and $\overline{\Delta p}$ is the steady pressure drop, then the relationship between the ensemble-averaged time-dependent parts $\langle U\rangle$ and $\langle \Delta p\rangle$ can be expressed by the equation

$$\frac{\langle U\rangle}{\overline{U}} = \frac{\langle Q\rangle}{\overline{Q}} = \sigma_q \frac{\langle \Delta p\rangle}{\overline{\Delta p}} \cos \phi_q,$$

where the amplitude coefficient $\sigma_q = ([\langle Q\rangle]/\overline{Q})/([\langle \overline{\Delta p}\rangle]/\Delta p)$ and the phase lag ϕ_q were calculated for fully developed laminar flow by Uchida (1956). At very low frequencies ($\alpha < 1$) $\sigma \approx 1$ and the phase lag $\phi_q \approx 0$. Thus, when the frequency of the imposed pulsations is low, the flow at any instant behaves like Poiseuille flow at the appropriate instantaneous pressure gradient. Inertia effects become noticeable with increasing frequency when the flow can no longer follow the rapid changes in pressure.

The mechanical power W necessary to push the flow at rate Q through a pipe in which the pressure drops by Δp is proportional to the product $Q\,\Delta p$. In pulsating flow the power is time-dependent, and the instantaneous power consumption is $W = (\overline{\Delta p} + \langle \Delta p\rangle)(\overline{Q} + \langle Q\rangle)$. Representing the oscillations in pressure and in flow rate by the corresponding amplitudes and phase angles and averaging over the period, one obtains:

$$\overline{W} = \overline{\Delta p} + [\langle \Delta p\rangle][\langle Q\rangle]\,\overline{\cos \omega t \cos(\omega t - \phi_q)}$$

$$= \overline{\Delta p\, Q} + 0.5[\langle \Delta p\rangle][\langle Q\rangle] \cos \phi_q.$$

The additional time-averaged power necessary to impose the pulsations on the steady flow is thus proportional to $[\langle \Delta p\rangle][\langle Q\rangle] \cos \phi_q$.

At a given frequency the phase angle ϕ_q is the main contributor to the difference in the time-averaged power consumption between laminar and turbulent flows. In laminar flow the phase angle hardly deviates from 90° (it changes from 85° at $T = 0.56$ s ($\alpha = 13.8$) to about 78° at $T = 2.4$ s ($\alpha = 6.6$)). In turbulent flow, a change

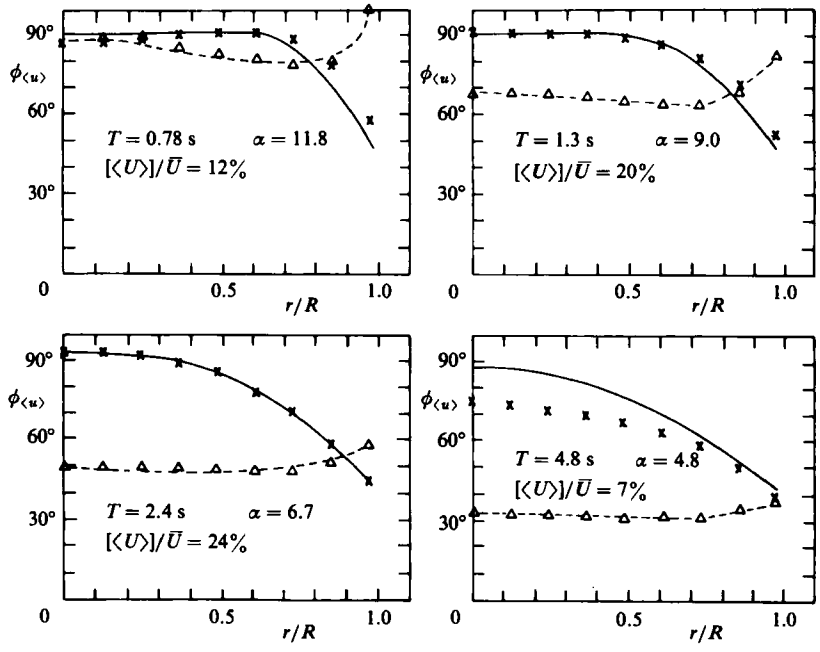

FIGURE 4. Radial distribution of ϕ_u in laminar and turbulent flows at $Re = 4000$: ×, measurements in laminar flow; △, measurements in turbulent flow. The solid line represents the theoretically calculated distribution in fully developed laminar flow.

in frequency causes a more significant decrease in the phase lag of the flow behind the pressure drop. At high frequencies there is only a small difference in ϕ_q between laminar and turbulent flows; at $T = 0.56$ s ϕ_q is about 85° in both cases. In turbulent flow ϕ_q decreases fast with decreasing frequency (at $T = 2.4$ s $\phi_q \approx 50°$), and $\cos\phi_q$ therefore becomes larger than in the corresponding laminar case.

In the absence of viscosity the pressure gradient, being the only driving force, is in phase with the acceleration of the fluid. The velocity lags 90° behind pressure. The radial distribution of the phase angle is shown in figure 4 for $Re = 4000$ and various periods of oscillations. The solid lines show the theoretical prediction of Uchida, while the crosses and the triangles give the measured phase angles in fully developed laminar and turbulent flows, respectively. A good agreement with the theory was obtained in the laminar case, with the exception of lowest frequency measured; in this case the influence of the entrance region becomes more pronounced (Shemer 1981). The phase lag on the centreline in laminar flow is usually 90°, decreasing to approximately 45° near the wall.

In turbulent flow the conditions are different. The dimensionless frequency $\alpha = (\omega/\nu)^{\frac{1}{2}}$ is no longer a controlling parameter because the molecular viscosity is irrelevant and could perhaps be replaced by an equivalent eddy viscosity ϵ_T, which is orders of magnitude larger than ϵ. The effective α is therefore much lower, and the phase lag of the velocity in the central region of the pipe decreases more quickly with the increasing period than in the corresponding laminar flow. In contrast to laminar flow, the phase lag in the wall region increases towards the wall. The qualitative nature of the result was noticed by Ramaprian & Tu (1980). Shemer & Wygnanski (1981) attributed this phenomenon to the relatively slow adaptation of the turbulence to the local flow conditions, manifested in this case in the phase lag of Reynolds stress

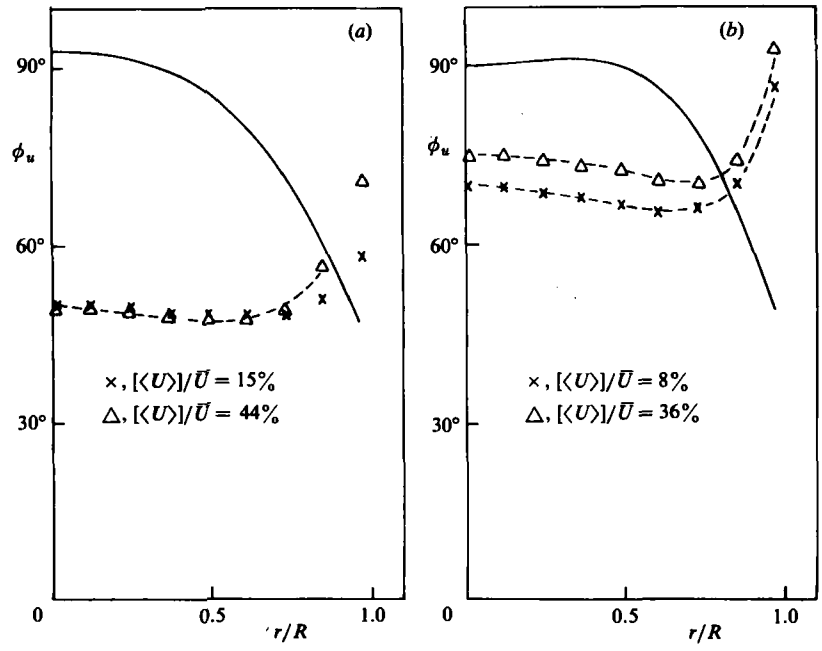

FIGURE 5. The dependence of ϕ_u on the amplitude of oscillations at $Re = 4000$. The solid line represents the theoretically calculated phase distribution in the corresponding fully developed laminar flow, (*a*) $T = 2.4$ s, (*b*) $T = 1.25$ s.

behind the radial derivative of the oscillating velocity component. This phase lag suggested that the effective eddy viscosity is a complex number. Calculation based on a model using complex eddy viscosity confirmed this suggestion.

The radial distribution of the phase lag in velocity in the turbulent flow depends on amplitude and on Reynolds number. The dependence on the amplitude of pulsations is rather weak. The radial distribution of the phase lag for two amplitudes of pulsations at two frequencies is presented in figures 5(*a*) and (*b*). At low frequency ($T = 2.4$ s) a change in amplitude caused no concomitant change in phase in the central region of the pipe. At higher frequency ($T = 1.25$ s) the influence of amplitude on the phase angle is felt across the entire cross-section. However, a large increase in amplitude results in a relatively small change in the phase angle (less than 5°). The linear dependence if the velocity amplitude on forcing (figure 3) and the independence of the radial distribution of ϕ_u on the forcing amplitude suggest that at sufficiently low amplitudes of forcing turbulent pulsating flow behaves in a linear manner.

The dependence of the phase angle on the mean Reynolds number in turbulent flow is more pronounced. A characteristic eddy viscosity increases with increasing *Re*, reducing effective α. The phase lag in velocity, therefore, decreases with increasing *Re* (figure 6). On the other hand, the viscous sublayer becomes thinner with increasing *Re*, and therefore the phase lag at $Re = 7500$ is practically constant across the pipe.

A qualitative difference between laminar and turbulent pulsating flows may be noticed in the radial distribution of the amplitude in the velocity oscillations. In laminar flow, these amplitudes attain a maximum within the Stokes layer near the wall, while in turbulent flow the maxima are shifted to the centre of the pipe

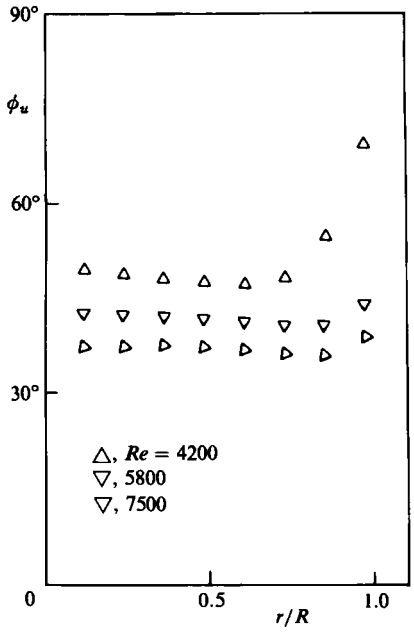

FIGURE 6

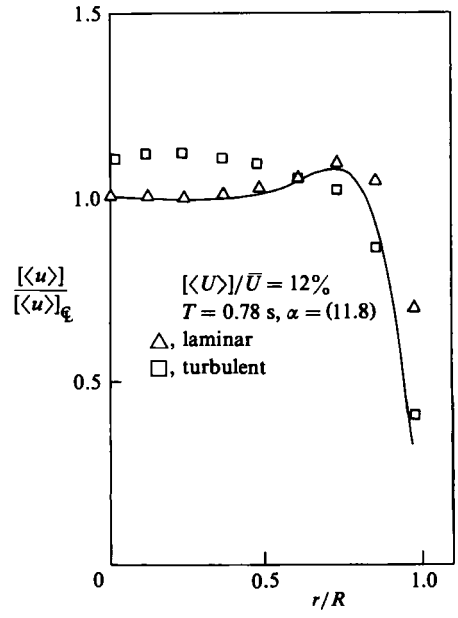

FIGURE 7

FIGURE 6. The dependence of ϕ_u on Re in turbulent flow at $T = 2.4$ s, $[\langle U\rangle]/\overline{U} \approx 20\%$.

FIGURE 7. The radial distribution of velocity amplitude in laminar and turbulent flows at $Re = 4000$. The solid line is the theoretically calculated distribution in laminar flow.

(figure 7). The theoretically calculated distribution of amplitudes in laminar flow (Uchida 1956) is shown also in figure 7 for comparison.

The amplitude distribution of the axial component of velocity in the turbulent flow is nearly uniform in the central region of the pipe, and decreases rapidly near the wall. Increasing the mean Re or decreasing the frequency of oscillations results in a more uniform distribution of the velocity amplitudes in turbulent flow. The reasons for this effect were already discussed in conjunction with the radial distribution of the phase lag.

3.3. *Turbulent-flow parameters*

3.3.1. *Turbulent velocity fluctuations*

The instantaneous axial (u) and radial (v) velocity components, measured during a single period, are shown and compared with their respective phase-averaged values in figure 8; the variation of pressure with time is shown above the velocities. One may observe that (i) the phase-averaged radial velocity component vanishes throughout, thus there are no Reynolds stresses associated with orderly pulsating part of the flow, and (ii) the amplitudes and the prevailing frequencies of the turbulent velocity fluctuations depend on the phase of the imposed oscillations.

The dependence of the turbulent activity on the phase of the forcing becomes more evident at higher amplitudes of pulsations. Oscillating velocities recorded at high amplitudes of excitation (figure 9) indicate a partial laminarization during the time corresponding to minimum velocity. A 'breakdown' to turbulence re-occurs when the instantaneous velocity is a maximum; at that time the amplitudes of the turbulent fluctuations increase suddenly. The decrease in the amplitude of the fluctuations on the decelerating portion of the cycle is relatively gradual.

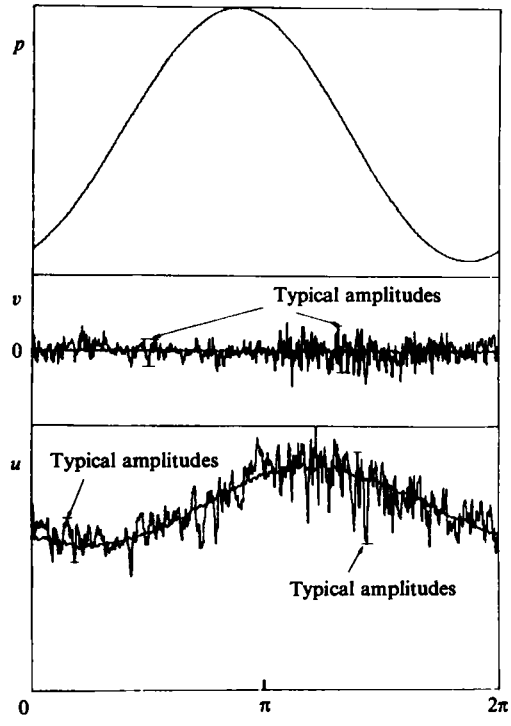

FIGURE 8. Single period measured by an x-wire probe and pressure transducer and compared with phase-averaged values ($Re = 4000$, $T = 1.34$ s, $r/R = 0$, $[\langle U\rangle]/\overline{U} = 20\,\%$).

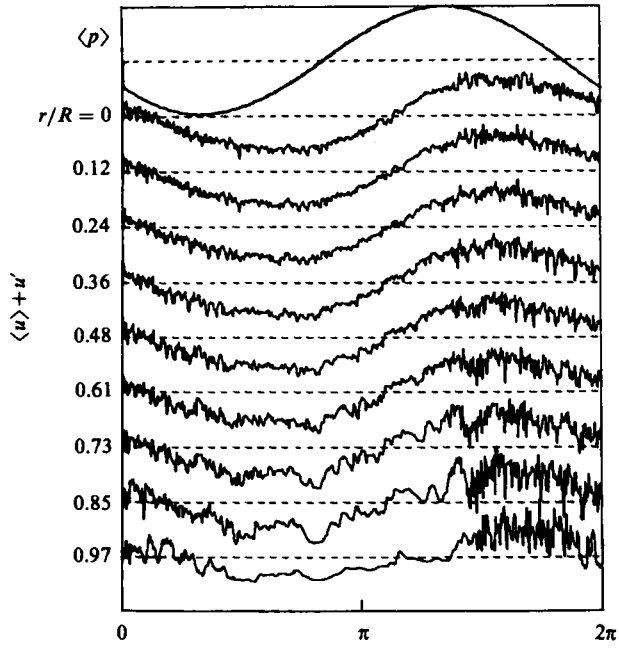

FIGURE 9. D.c. filtered single period, measured by the rake of 9 hot wires ($Re = 4000$, $T = 2.4$ s, $[\langle U\rangle]/\overline{U} = 44\,\%$).

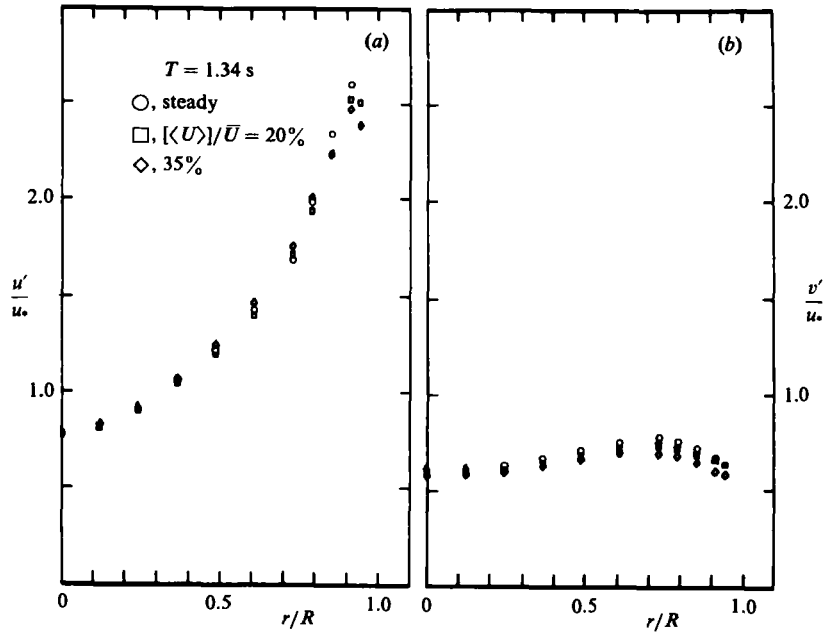

FIGURE 10. The radial distribution of r.m.s. values of turbulent velocity fluctuations at $Re = 4000$; (*a*) in streamwise direction; (*b*) in radial direction.

Increasing further the amplitudes of pulsations results in complete relaminarization of the flow whenever the duration at a subcritical Re is sufficiently long and no additional disturbances are introduced downstream. The mean velocity of the flow at $Re = 4000$ is only 1.8 m/s, so that even at the lowest frequency of pulsations ($T = 4.5$ s) the residence time of the fluid in the pipe spans several periods. Because the flow is naturally laminar at $Re = 4000$, turbulence was triggered artificially by a protuberance placed at the entrance to the pipe. Thus, if the flow relaminarizes because the instantaneous Re falls below its critical value during a fraction of the period, it will remain laminar throughout the rest of the pipe. The effect of relaminarization of the initially turbulent flow at low Reynolds numbers due to imposed pulsations was noticed by number of investigators (e.g. Ramaprian & Tu 1980). It should be stressed that the experimental results presented in this paper are restricted to relatively low amplitudes of forcing (less than 35% of the flow rate) in order to avoid relaminarization. Transitional flow will be discussed separately.

The radial distributions of the time-averaged, r.m.s. values of turbulent fluctuations in the axial and radial directions for steady and pulsating flows are compared in figure 10. The velocity fluctuations are normalized by the friction velocity u_* which was calculated from the time-averaged pressure drop ($u_* = 13.1$ cm/s at $Re = 4000$). There is no significant difference between mean values of $\overline{u'^2}$ and $\overline{v'^2}$ in steady and pulsating flows. The distribution of $\overline{u'^2}$ and $\overline{v'^2}$ is in good agreement with earlier measurements made by Wygnanski & Champagne (1973) at comparable Reynolds number in steady flow. In the steady turbulent flow the normalization of u' by friction velocity u_* is most appropriate. In many cases, however, bulk velocity $\bar{U}$, or the velocity on the centreline of the pipe are used for the sake of convenience. This can be justified by the weak dependence of $u_*/\bar{U}$ on the Reynolds number, which stems from the fact that in turbulent flow the shear stress at the wall $\bar{\tau}_w$ is almost

proportional to $\overline{U}^2$, resulting in $u_* \sim \overline{U}$; in fact, any double velocity correlation $\overline{u_i' u_j'}$ is proportional to $\overline{U}^2$. Assuming the same relation for slowly varying turbulent periodic flows in which the turbulent structure has adequate time to adjust to the instantaneous distribution of velocity, we obtain:

$$\frac{\tau_w}{\rho} = \frac{\bar{\tau}_w + \langle \tau_w \rangle}{\rho} \propto (\overline{U} + \langle U \rangle)^2 \approx \overline{U}^2 + 2\overline{U}\langle U \rangle, \tag{3}$$

provided that the amplitude of the pulsations in the bulk velocity $[\langle U \rangle]$ is small (i.e. $[\langle U \rangle]/\overline{U} \ll 1$). The amplitude of the time-dependent portion of the friction velocity $[\langle u_* \rangle]$ can be expressed by:

$$[\langle u_* \rangle]^2 = \frac{[\langle \tau_w \rangle]}{\rho} \propto 2\overline{U}[\langle U \rangle],$$

which is analogous to the steady flow where $u_*^2 = \tau_w/\rho \propto \overline{U}^2$. The amplitude of an oscillation in $\langle u_i' u_j' \rangle$ can therefore be normalized by $[\langle u_* \rangle]^2$. Thus, for quasi-steady flow the following relation holds:

$$\frac{\langle u_i' u_j' \rangle}{2\overline{U}[\langle U \rangle]} = \frac{\overline{u_i' u_j'}}{\overline{U}^2}, \tag{4}$$

where $[\langle u_i' u_j' \rangle]$ is the amplitude of the oscillations in the corresponding velocity correlation. It seems reasonable to normalize the amplitudes of $\langle u_i' u_j' \rangle$ by $2\overline{U}[\langle U \rangle]$ and compare them with $\overline{u_i' u_j'}/\overline{U}^2$. Any discrepancy between the radial distribution of $[\langle u_i' u_j' \rangle]$ normalized in this manner and the time-averaged value indicates that the unsteady flow influences the turbulent structure.

The ratio of $[\langle u'^2 \rangle]/2\overline{U}[\langle U \rangle]$ for three forcing periods at identical amplitudes of $[\langle U \rangle]/\overline{U} \approx 15\,\%$, is compared to the steady radial distribution of $\sqrt{\overline{u'^2}}/\overline{U}$ in figure 11. At high frequency ($T = 0.78$ s) the normalized value of $[\langle u'^2 \rangle]$ is higher than the corresponding time-averaged value while at low frequencies $[\langle u'^2 \rangle]$ is lower than $\overline{u'^2}$. The radial distributions of $[\langle u'^2 \rangle]/2\overline{U}[\langle U \rangle]$ and of $\sqrt{\overline{u'^2}}/\overline{U}$ are similar; some differences between the two may be observed in the wall region. It follows from (4) that in a quasi-steady flow $\overline{U}[\langle u'^2 \rangle]/2\overline{u'^2}[\langle U \rangle] = 1$. Since $\overline{u'^2}$ is independent of periodic surging (figure 10), the results of figure 11 indicate that this last equation is approximately correct. The differences between the normalized distributions of $[\langle u'^2 \rangle]$ at lowest frequency and $\overline{u'^2}$ are discussed in Shemer & Kit (1984).

The dependence of $([\langle u'^2 \rangle])^{\frac{1}{2}}/2\overline{U}[\langle U \rangle]$ on the amplitude of bulk velocity $[\langle U \rangle]$ is rather weak (figure 12*a*). The data presented in this figure reflect a variation of 300 % in the amplitude of excitation, which resulted in a 10 % change in $[\langle u'^2 \rangle]$. In figure 12 (*a*) a comparison is shown between measurements made with a rake of normal wires and measurements made with an X-wire at identical flow conditions ($T = 1.34$ s, $[\langle U \rangle]/\overline{U} = 20\,\%$). There is reasonable agreement between the two sets of data.

The radial distributions of $([\langle v'^2 \rangle]/2\overline{U}[\langle U \rangle])^{\frac{1}{2}}$ for two amplitudes of the bulk velocity are compared with the time-mean distribution in figure 12 (*b*). No significant dependence of $[\langle v'^2 \rangle]/2\overline{U}[\langle U \rangle]$ on the amplitude can be noticed. The measured values of dimensionless amplitude $[\langle v'^2 \rangle]$ are slightly higher than the corresponding time-averaged value, but the radial distributions of $([\langle v'^2 \rangle]/2\overline{U}[\langle U \rangle])^{\frac{1}{2}}$ and $(\overline{v'^2})^{\frac{1}{2}}/\overline{U}$ are very similar. The amplitude of the turbulent fluctuations in the streamwise direction increases rapidly with r up to $r/R = 0.95$, while the amplitude of the radial fluctuations is nearly independent of the radius.

Figures 13 (*a*)–(*c*) show the radial distribution of phases of $\langle u'^2 \rangle$ and $\langle u \rangle$ for three forcing periods ($0.78\text{ s} \leqslant T \leqslant 2.4$ s) at a constant amplitude of excitation

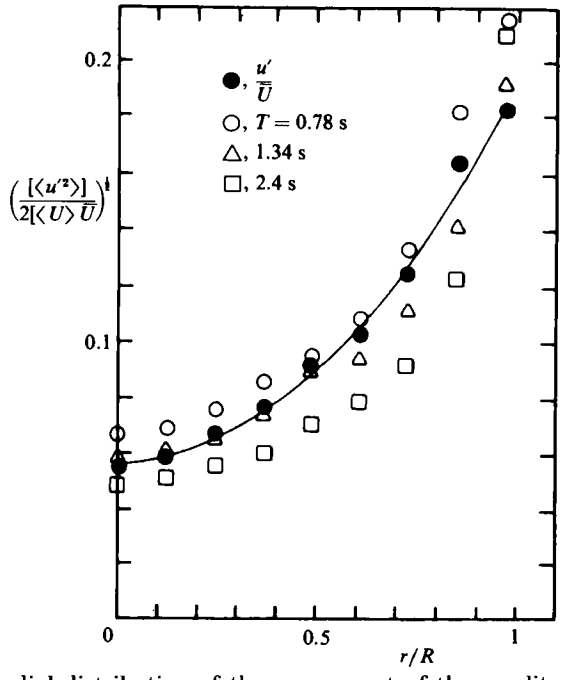

FIGURE 11. The radial distribution of the square root of the amplitude of pulsations in u'^2 at $Re = 4000$ and $[\langle U\rangle]/\bar{U} \approx 15\%$ at various frequencies of forcing. The solid line is the corresponding distribution of the r.m.s. values of velocity fluctuations in steady flow.

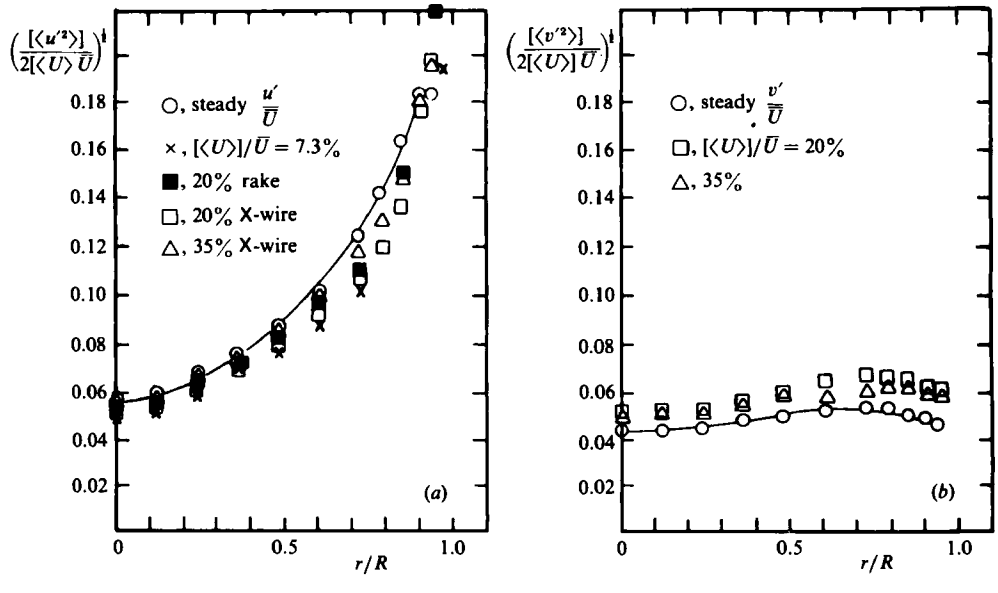

FIGURE 12. The radial distribution of the square root of the amplitude of pulsations in the velocity fluctuations at $Re = 4000$ and $T = 1.34$ s at various amplitudes of forcing. The solid line is the corresponding distribution of the r.m.s. values of velocity fluctuations in steady flow: (*a*) in streamwise direction; (*b*) in radial direction.

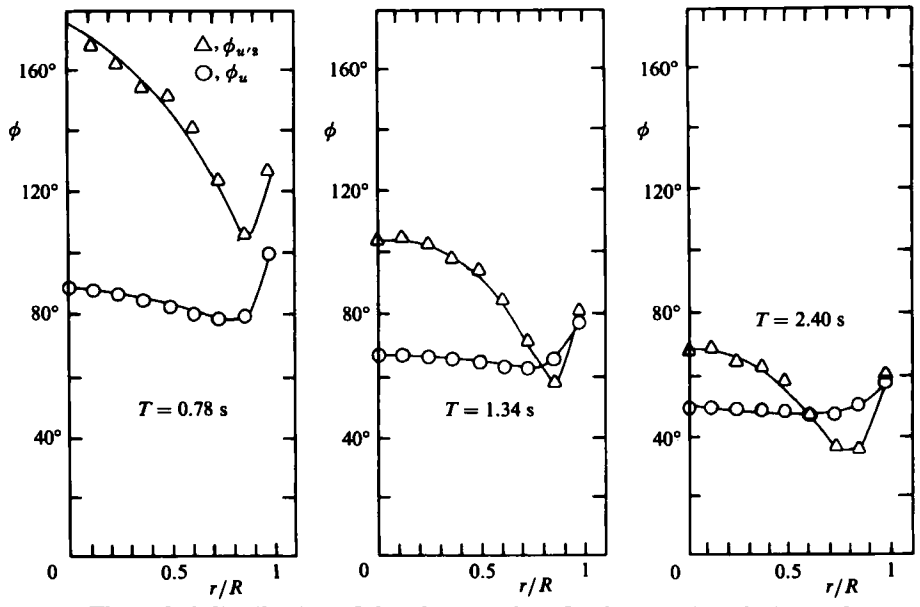

FIGURE 13. The radial distribution of the phase angles of pulsations in velocity and in turbulent intensity in a streamwise direction at $Re = 4000$, $[\langle U\rangle]/\overline{U} \approx 15\,\%$ and at various frequencies of forcing.

($[\langle U\rangle]/\overline{U} \approx 15\,\%$). The angle between $\langle u'^2\rangle$ and $\langle u\rangle$ increases with increasing frequency. The phase angle of $\langle u'^2\rangle$ depends strongly on radial position, being a maximum at the centre of the pipe, and attaining a minimum in the region in which turbulent production is a maximum. ϕ_u is almost constant in the central core of the pipe. At lower frequencies ($T > 1$ s) $\phi_{u'^2}$ at $r/R \approx 0.7$ actually leads the phase of $\langle u\rangle$. The effects of Re on the radial distributions of ϕ_u and $\phi_{u'^2}$ can be assessed from figure 14. The Reynolds numbers considered vary from 3900 to 7500. The radial distribution of $\phi_{u'^2}$ becomes more uniform with increasing Re; the location of the minimum in the radial distribution of $\phi_{u'^2}$ moves towards the wall with increasing Re, as does the region of maximum production.

The phase angle of $\langle v'^2\rangle$ is almost independent of the radial position (figure 15). $\phi_{v'^2}$ is very close to $\phi_{u'^2}$ in the centre of the pipe, but it does not decrease at larger r/R. The magnitude of the phase lag in $\langle u'^2\rangle$ and $\langle v'^2\rangle$ in relation to the pulsating velocity $\langle u\rangle$ depends slightly on the amplitude of the forcing, but the general shape of the radial distribution of the phase is not affected by the increase in the amplitude.

In order to check whether $\langle u'^2\rangle$ and $\langle v'^2\rangle$ can be represented by a simple harmonic function at the fundamental frequency of forcing f_0 the ratio of the first two power-spectral coefficients $c(2f_0)/c(f_0)$ was calculated for the phase-averaged r.m.s. values. This ratio was about 3% for $[\langle U\rangle]/\overline{U} = 15\,\%$, and increased to 16% at $[\langle U\rangle]/\overline{U} = 35\,\%$. The non-harmonic distortion did not show significant dependence on the radial location. The non-harmonic behaviour of $\langle v'^2\rangle$ was similar.

3.3.2. *Reynolds stress*

Time-averaged Reynolds stresses $-\overline{u'v'}/\overline{U}^2$ (figure 16) are also independent of the imposed oscillations. This was inferred earlier from the similarity of the time-averaged velocity profiles (see figure 2). Normalization of $[\langle u'v'\rangle]$ by $2\overline{U}[\langle U\rangle]$ (figure 17) indicates that the amplitudes of the Reynolds stress are insensitive to the amplitude

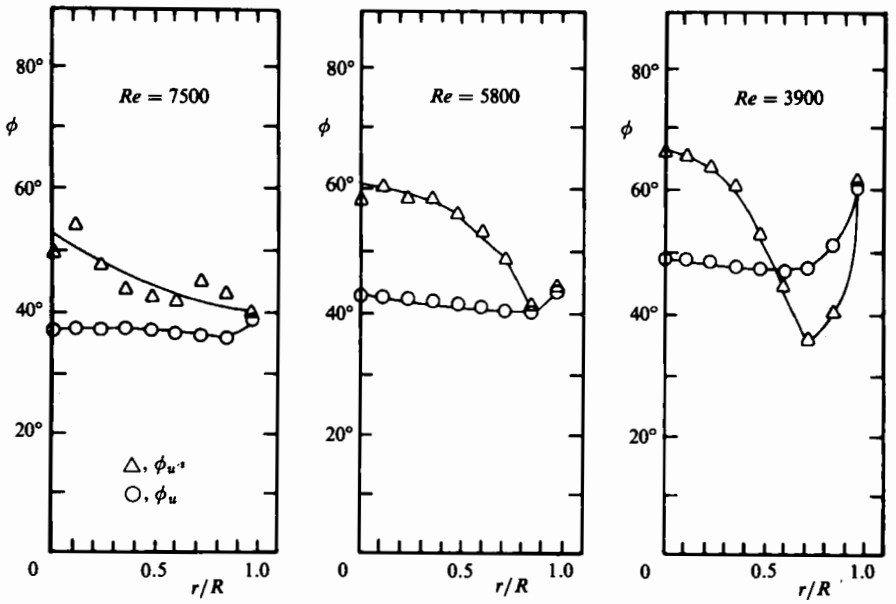

FIGURE 14. The radial distribution of the phase angles of pulsations in velocity and turbulent intensity in streamwise direction at various Reynolds numbers and $[\langle U\rangle]/\bar{U} \approx 10\%$; $T = 1.6$ s.

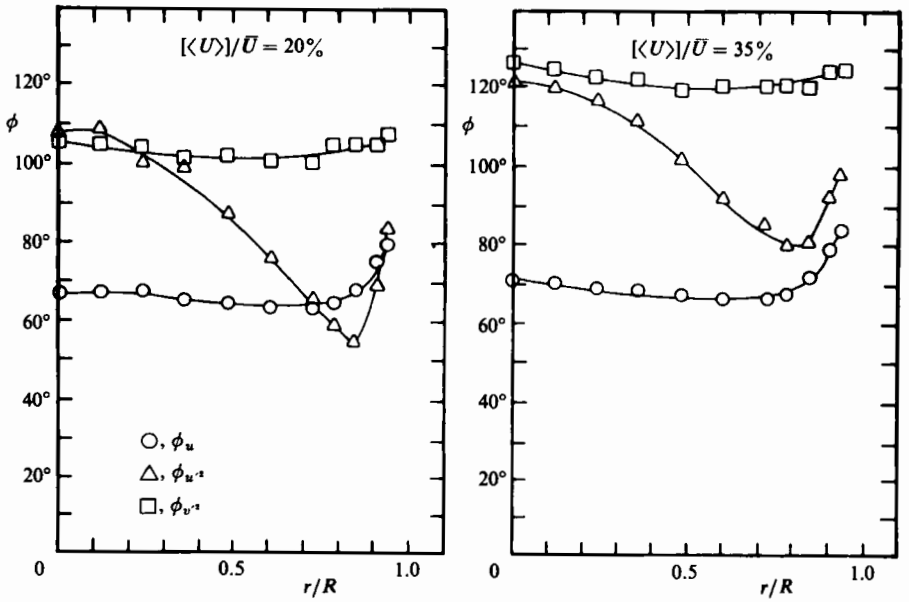

FIGURE 15. The radial distribution of phase angles of pulsations in velocity and in turbulent fluctuations in streamwise and radial directions at $Re = 4000$ and $T = 1.34$ s.

of the pulsating bulk velocity. Qualitatively, the radial distribution of $[\langle u'v'\rangle]$ resembles the time-averaged $\overline{u'v'}$ distribution; both grow linearly with the radius in the central region of the pipe, but the pulsating $[\langle u'v'\rangle]$ attains its maximum somewhat closer to the wall than the time-averaged Reynolds stress. The normalized values of $[\langle u'v'\rangle]$ are higher than the corresponding time-averaged Reynolds stresses, as is also the case with $[\langle v'^2\rangle]$ (figure 12*b*).

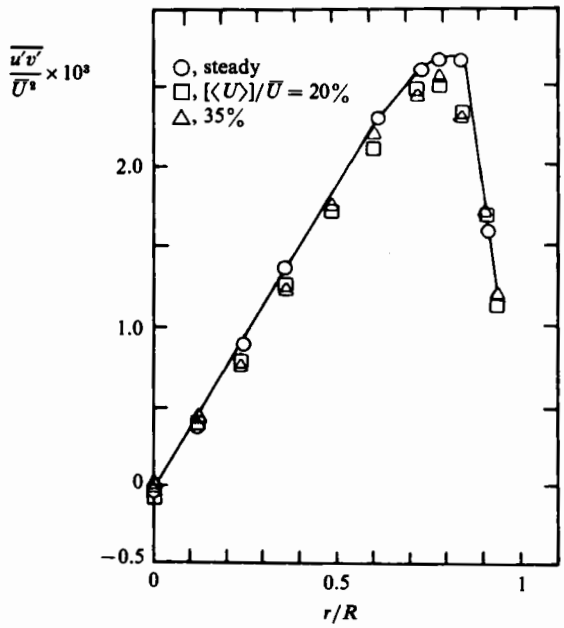

FIGURE 16. The radial distribution of the time-averaged Reynolds stress at $Re = 4000$ in steady and pulsating flows ($T = 1.34$ s).

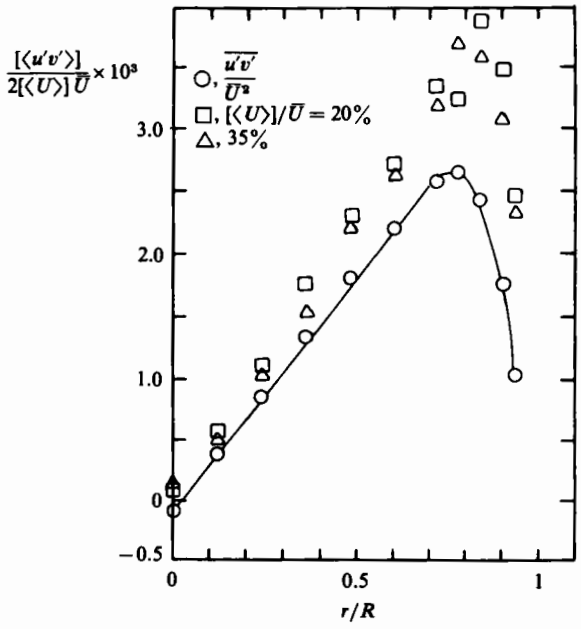

FIGURE 17. The amplitude of pulsations in the Reynolds stress at $Re = 4000$ and $T = 1.34$ s, compared to the time-averaged distribution.

The radial distribution of $\phi_{u'v'}$ relative to the pressure (figure 18) lies between the phase of $\langle u'^2 \rangle$ and $\langle v'^2 \rangle$ at the corresponding amplitudes of the bulk velocity and radial positions (compare with figure 15). The phase angle of $\langle u'v' \rangle$ is equal to $\phi_{u'^2}$ and $\phi_{v'^2}$ in the central region of the pipe and attains a minimum near the wall (at $0.7 < r/R < 0.8$). The location of this minimum depends on the amplitude of forcing.

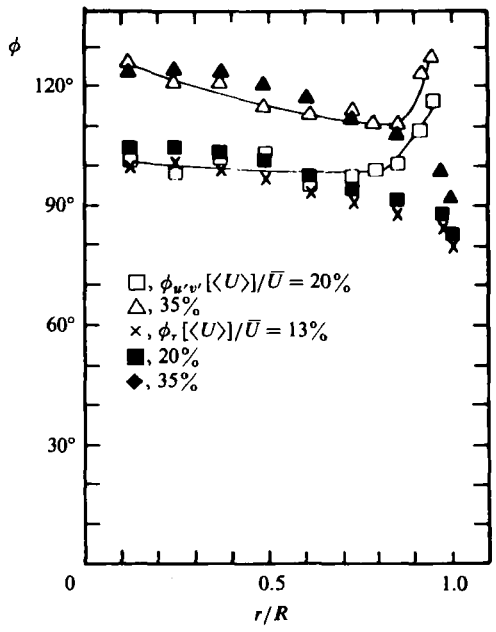

FIGURE 18. The radial distribution of the phase angle of the shear stress and the Reynolds stress at $Re = 4000$, $T = 1.34$ s and various amplitudes of forcing.

As a check on the harmonic behaviour of the Reynolds stresses, the 'power spectrum' of the phase-averaged $\langle u'v' \rangle$ was calculated, and the coefficients corresponding to the fundamental frequency and its first harmonic were compared. Their ratio was found to be similar to the ratio of coefficients estimated for $\langle u'^2 \rangle$ (i.e. $c(f_0)/c(2f_0) \approx 4\%$ when the amplitude of forcing was 20%; and 16% when $[\langle U \rangle]/\bar{U} = 35\%$).

3.3.3. *The balance of forces in a pulsating flow*

In a steady fully developed pipe flow there are two types of forces acting on every element of fluid and balancing one another: pressure forces, resulting from a favourable pressure gradient in the direction of the flow; and shear forces caused by friction with the walls and acting in the opposite direction. In a non-steady flow an inertia has to be considered. All three forces have to be balanced at every instant, forming a triangle of forces for each frequency in the Fourier expansion. Only the leading term, at the fundamental frequency of pulsations, is considered here.

The time-dependent part of the moment equation has the following form:

$$\frac{\partial \langle u \rangle}{\partial t} = -\frac{1}{\rho}\frac{\partial \langle p \rangle}{\partial x} + \frac{1}{r\rho}\frac{\partial}{\partial r}(r\langle \tau(r) \rangle), \tag{5}$$

where $\langle \tau \rangle$ is the ensemble-averaged pulsating part of the shear stress given by

$$\langle \tau \rangle = \mu \frac{\partial \langle u \rangle}{\partial r} - \rho \langle u'v' \rangle. \tag{6}$$

Integrating (5) from the centreline to another radial position r yields

$$\frac{\rho}{r^2}\frac{\partial}{\partial t}\int_0^r r' \langle u(r') \rangle \, dr' = -\frac{1}{2}\frac{\partial \langle p \rangle}{\partial x} + \frac{\langle \tau(r) \rangle}{r}. \tag{7}$$

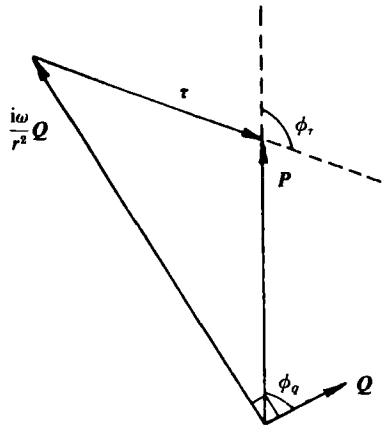

FIGURE 19. The balance of forces in pulsating flow.

The integral on the left-hand side represents an instantaneous flow rate through the central region of the pipe up to the radial position r: $\langle Q(r)\rangle = 2\pi\int_0^r r'\langle u(r')\rangle\,\mathrm{d}r'$. It is convenient to define $\boldsymbol{P}$, $\boldsymbol{Q}(r)$ and $\boldsymbol{\tau}(r)$ in the complex form:

$$\left.\begin{aligned} \boldsymbol{P} &= -\frac{1}{\rho}\frac{\partial\langle p\rangle}{\partial x} = [\langle P\rangle]\exp(\mathrm{i}\omega t),\\ \boldsymbol{Q}(r) &= [\langle Q(r)\rangle]\exp\{\mathrm{i}(\omega t-\phi_q(r)\},\\ \text{and}\qquad \boldsymbol{\tau}(r) &= -\frac{2[\langle\tau(r)\rangle]}{\rho r}\exp\{\mathrm{i}(\omega t-\phi_\tau(r)\}, \end{aligned}\right\} \tag{8}$$

where the negative sign in the definition of $\boldsymbol{\tau}(r)$ is introduced for convenience, giving in the quasi-steady flow with negligible inertia the value of the phase angle $\phi_\tau \to 0$. For the fundamental frequency, the differential equation (7) reduces to an algebraic expression

$$\frac{\mathrm{i}}{\pi}\frac{\omega}{r^2}[\langle Q(r)\rangle]\exp\{-\mathrm{i}\phi_q(r)\}+\frac{2[\langle\tau(r)\rangle]}{\rho r}\exp\{-\mathrm{i}\phi_\tau(r)\} = [\langle P\rangle]. \tag{9}$$

The amplitude of the shear stress $[\langle\tau(r)\rangle]$ and its phase angle ϕ_τ can be evaluated from (9) provided that the experimental information about flow velocities and pressure is available.

Taking into account that in turbulent flow the mass flux lags behind the pressure by an angle ranging from 0° to 90°, depending on frequency and Reynolds number, figure 19, representing (9), can be drawn.

The shear stresses calculated from (9) can therefore be checked experimentally. The calculated radial distributions of $[\langle\tau\rangle]/\rho$, normalized by $2\overline{U}[\langle U\rangle]$, are shown in figure 20. Three different amplitudes of pulsations are considered at a single period of $T = 1.34$ s. It is seen that the suggested normalization leads to radial distributions of $[\langle\tau\rangle]/2\rho\overline{U}[\langle U\rangle]$ which collapse fairly well on a single curve. The comparison between the measured Reynolds stress (figure 17) and calculated stress using (9) is satisfactory except in the wall region where the viscous term in (6) becomes important. In the central region of the pipe $-\partial\langle u\rangle/\partial r \approx 0$, and therefore $-\langle\tau\rangle/\rho = \langle u'v'\rangle$, yet the measured values of $[\langle u'v'\rangle]$ are consistently lower than $[\langle\tau\rangle]/\rho$. The maximum discrepancy, however, is about 15% (figure 20), giving an

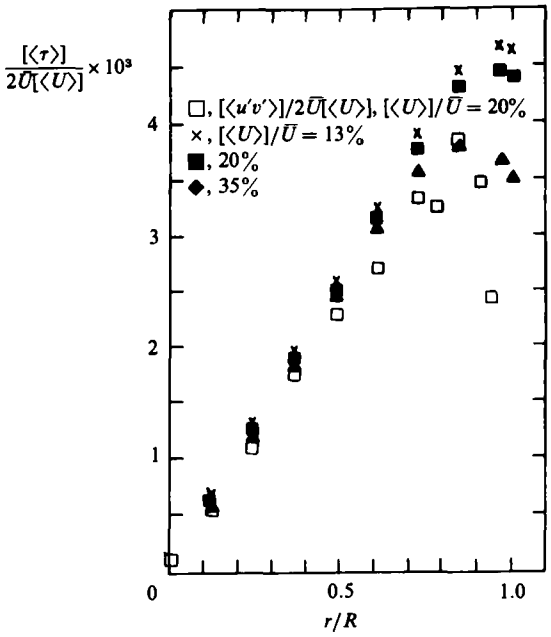

FIGURE 20. The amplitude of pulsations in the shear stress at $Re = 4000$, $T = 1.34$ s and various amplitudes of forcing, compared with the radial distribution of the amplitude of pulsations in the Reynolds stress.

estimate of the possible error resulting from the use of experimentally measured velocities and pressure gradients in (9).

The dependence of $[\langle\tau\rangle]/2\rho\bar{U}[\langle U\rangle]$ on the frequency of forcing is shown in figure 21. Changing the frequency of the imposed oscillations affects the shape and the magnitude of the radial distribution of $[\langle\tau\rangle]$; in the central region of the pipe the slope of this quantity with respect to the radial distance from the centre increases with frequency, but the location at which it attains a maximum occurs farther from the wall than at lower frequencies. At the lowest frequency, $[\langle\tau\rangle]$ is proportional to the radial position up to the largest r/R measured, thus behaving like the radial distribution of the time-averaged shear stress.

A phase difference exists between the oscillations in flow rate and in shear stress. The phase lag of $\langle\tau\rangle$, ϕ_τ, as calculated from (9), shows only slight dependence on amplitude (figure 18), with one exception corresponding to the highest amplitude of forcing ($[\langle U\rangle]/\bar{U} \approx 35\%$). The calculated values of ϕ_τ are compared in figure 18 with directly measured $\phi_{u'v'}$ at identical amplitudes of forcing. The agreement between the corresponding distributions of ϕ_τ and $\phi_{u'v'}$ in the central region of the pipe is good, providing additional verification for the calculated values of $\langle\tau\rangle$. The values of ϕ_τ and $\phi_{u'v'}$ are quite different in the wall region where the viscous part of the shear stress becomes important; ϕ_τ decreases towards the wall while $\phi_{u'v'}$ increases (figure 18). The decrease in ϕ_τ is more pronounced at higher frequencies (figure 22). The phase lag of the shear stress behind the pressure is strongly dependent on frequency. Even at the lowest frequency of pulsations ($T = 4.5$ s) there is still a considerable phase angle between $-\langle\tau\rangle$ and $-\langle\partial p/\partial x\rangle$, in spite of the fact that the phase difference between $-\langle\tau\rangle$ and $\langle u\rangle$ vanishes (figure 22). Thus, for the purpose of force balance, the lowest frequency of excitation used in this experiment is not low enough for the flow to be considered quasi-steady.

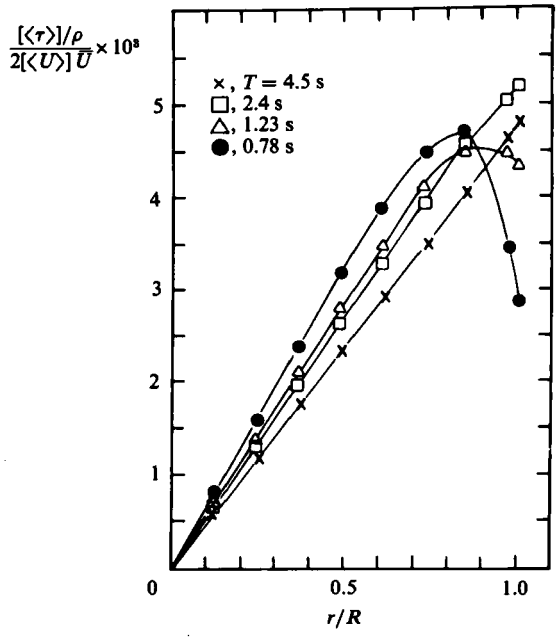

FIGURE 21. The amplitude of pulsations in the shear stress at $Re = 4000$, $[\langle U\rangle]/\overline{U} \approx 10\%$ and various frequencies of forcing.

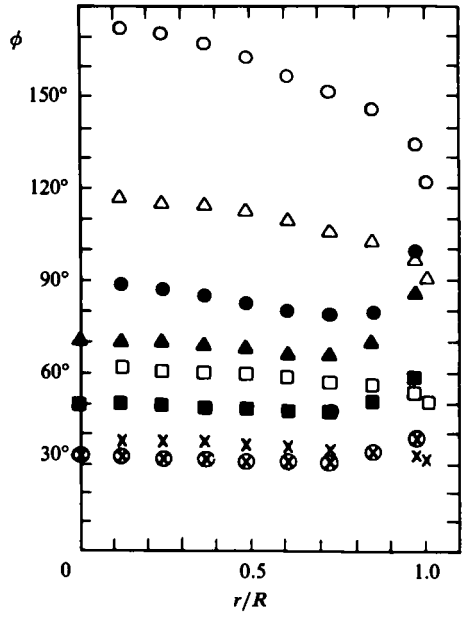

FIGURE 22. The phase angles of the pulsations in the shear stress and in the axial velocity at $Re = 4000$, $[\langle U\rangle]/\overline{U} \approx 10\%$ and various frequencies of forcing: ○, ϕ_τ, $T = 0178$ s; ●, ϕ_u, $T = 0.78$ s; △, ϕ_τ, $T = 1.23$ s; ▲, ϕ_u, $T = 1.23$ s; □, ϕ_τ, $T = 2.40$ s; ■, ϕ_u, $T = 2.40$ s; ×, ϕ_τ, $T = 4.50$ s; ⊗, ϕ_u, $T = 4.50$ s.

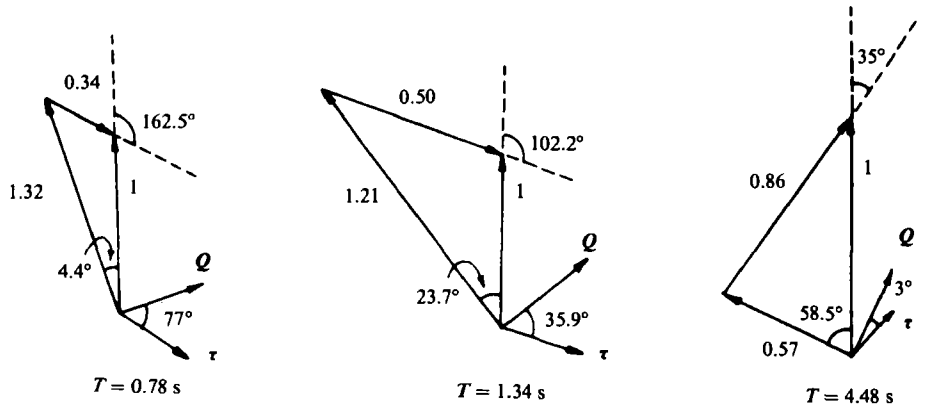

FIGURE 23. Force triangles at $r/R = 0.61$, $[\langle U\rangle]/\overline{U} \approx 15\%$ and three frequencies of forcing ($Re = 4000$).

The calculated values of $[\langle\tau\rangle]$ and ϕ_τ can be used to illustrate the balance of forces in the pulsating flow by drawing vector diagrams. Figure 23, which cannot be drawn to scale, shows relevant vectors at a given radial location ($r/R = 0.61$) for three frequencies of excitation (all vector moduli are normalized by the modulus of $\boldsymbol{P}$), as calculated from experimental data in accordance with (9). Increasing the frequency results in a smaller phase angle between the pressure and the acceleration vector. The length of $\boldsymbol{Q}$ relative to the pressure decreases with increasing frequency but the product $\omega[\langle Q\rangle]$, which corresponds to the acceleration vector, increases with frequency. The angle between $\boldsymbol{\tau}$ and $\boldsymbol{P}$ increases with increasing frequency, as shown in figure 23. At a given radial position there is no practical difference between $-\langle\tau\rangle/\rho$ and $\langle u'v'\rangle$. The phase angle of $-\langle\tau\rangle$ may thus be considered equal to the phase angle of the Reynolds stress. The Reynolds stress hardly lags behind the flow rate at low frequencies, but this phase lag attains approximately 80° at $T = 0.78$ s. At high frequencies, the Reynolds stress nearly opposes the acceleration vector.

4. Discussion

The radial distribution of $[\langle u'^2\rangle]$, $[\langle v'^2\rangle]$, $[\langle u'v'\rangle]$, and $[\langle\tau\rangle]/\rho$, normalized by $2\overline{U}[\langle U\rangle]$, are in fair agreement with the radial distribution of the corresponding time-averaged parameters, normalized by $\overline{U}^2$. Consequently, the linearized dimensionless quantities chosen are physically sound. There are, however, some differences dependent on the frequency of forcing, which should be discussed in detail.

It seems reasonable to begin with the Reynolds stress, because this is the only turbulent quantity appearing in the time-averaged momentum equation for the fully developed turbulent pipe flow (Reynolds equation), and hence is directly related to the mean quantities. As can be seen by comparing figure 18 with figure 15, $\langle u'v'\rangle$ is lagging behind $\langle u\rangle$ at all radial positions.

The most probable reason for this phase lag is the slow adaptation (or relaxation) of turbulence to instantaneous mean shear. It is natural to assume that turbulence possesses 'memory' (Nee & Kovasznay 1969; Narasimha & Prabhu 1972) and responds to a change in the mean flow after some delay. Shemer & Wygnanski (1981) proposed a simple model for the time-dependent turbulent flow in which eddy viscosity for the oscillating part was represented by a complex number, thus

accounting for the experimentally observed phase difference between $\langle \partial u/\partial r \rangle$ and $\langle u'v' \rangle$. Calculations based on this model gave qualitatively the correct distribution $\phi_u(r)$ in turbulent pulsating flow.

Reynolds stresses were measured directly in one experiment in which the frequency was held constant. In that case, the calculated value of the oscillating part of the shear stress $-\langle \tau \rangle/\rho$ was almost equivalent to the Reynolds stress in the central region of the pipe. At low frequency ($T = 4.5$ s), the rate of change in the bulk velocity is slow, thus allowing accommodation of the turbulent structure to the phase-locked velocity distribution. This conclusion was drawn from comparison of the phase angles of the shear stress ϕ_τ measured at various frequencies with ϕ_u (both shown in figure 22). The changes in the turbulent characteristics of the flow are therefore in phase with the mass flux and the pulsating Reynolds number.

It can be seen from the vector triangles (figure 23) that the phase lag between mass flux and the pressure drop tends to 90° as the frequency increases, and all three vectors in the force triangle become collinear. Under these conditions the Reynolds stresses, which differ from $\langle \tau \rangle/\rho$ only in the vicinity of the wall, lag behind the mass flux by 90°. At sufficiently high frequencies, a minimum in the turbulent activity corresponds to a maximum in acceleration.

The radial distributions of phase angles of $\langle u'^2 \rangle$ and $\langle u'v' \rangle$ are similar. Contrary to Reynolds stress, $\langle u'^2 \rangle$ was measured twice, once with x-wire and the second time with the rake of normal wires at various amplitudes and frequencies of forcing. The oscillations in u'^2 usually lag behind $\langle u \rangle$; the phase angle of $\langle u'^2 \rangle$ is strongly dependent on the radial position and attains a minimum in the region where the production of turbulent energy is maximum. In this region, however, $\langle u'^2 \rangle$ may even lead $\langle u \rangle$.

The rate of change in the intensity of the longitudinal velocity fluctuations (i.e. $\partial \langle u'^2 \rangle/\partial t$) is governed by the product of the Reynolds stress and the velocity gradient. The temporal change in the phase-averaged velocity gradient produces a most pronounced change in $\langle u'^2 \rangle$, where the product of the Reynolds stress with $-\partial u/\partial r$ attains maximum. The phase difference between $\langle u \rangle$ and $\langle u'^2 \rangle$ is thus minimal in the region of maximum production, which occurs at approximately $r/R = 0.7$ at these Reynolds numbers. Once generated, the longitudinal velocity fluctuations diffuse across the pipe causing the phase difference between $\langle u \rangle$ and $\langle u'^2 \rangle$ to increase with increasing distance from the region of maximum production. Maximum phase lag occurs in the central core of the pipe where there is no direct production of the turbulent energy. The radial velocity fluctuations do not extract energy directly from the mean flow, but rather through pressure–velocity correlations; therefore they are less likely to be affected by local changes in the mean velocity. Thus, $\phi_{u'^2}$ is similar to $\phi_{v'^2}$ in the centre of the pipe, where both components acquire their energy via a diffusion process; however, $\phi_{v'^2}$ remains independent of radial location. The relaxational mechanism proposed by Shemer & Wygnanski (1981) accounts for the frequency dependence of $\phi_u - \phi_{u'^2}$ in the central region of the pipe. A decrease in relaxation time may also be responsible for the decrease in phase difference between $\langle u \rangle$ and $\langle u'^2 \rangle$ with increasing Reynolds number (figure 14) (see also Laufer & Badri Narayanan 1971). At fairly low frequencies ($T > 1$ s) and low Reynolds numbers $\langle u'^2 \rangle$ may lead $\langle u \rangle$ at certain radial locations instead of lagging behind as it does at higher frequencies ($T = 0.78$ s). In the limiting case of very low frequency, a quasi-steady flow is established for which the phase difference between $\langle u'^2 \rangle$ and $\langle u \rangle$ has to vanish at all radial positions.

The proposed normalization suggests that the radial distribution of the amplitudes

for the double-velocity correlations at a single point have to coincide with their normalized distribution for steady flow when the frequencies considered are very low. At the other extreme, at very high frequencies when the period of pulsations is shorter than the characteristic response time of the turbulent structure, the relaxational approach leads to the conclusion that the oscillations in the turbulent quantities have to vanish; thus the turbulence in this limiting case becomes independent of the phase angle. Brown, Margolis & Shah (1969) measured the oscillating skin-friction factor at very high frequencies (up to 3000 Hz) and realized that with increasing frequency the dependence of the friction factor on frequency tends to the laminar case. They concluded that the turbulence becomes 'frozen' and the oscillating part of the flow exhibits laminar-like behaviour. The present experimental results indicate that the amplitude of oscillations in $\langle u'^2 \rangle$ increases with increasing frequency and may exceed the time-mean values of $[\langle u \rangle]$ at higher frequencies (figure 11). The absolute differences are not large and may be partially attributed to the inaccuracy in the assumption that $u_i' u_j' \propto \overline{U}^2$, as well as to an experimental error. Nevertheless, dependence of the amplitude distribution on frequency contradicts some prevailing concepts. The same holds true with regards to the amplitudes of the shear stress in the central region of the pipe, where the influence of viscosity is negligible and the Reynolds stress is the main contributor to $\langle \tau \rangle$. The relaxational mechanism has to 'freeze' the Reynolds stress at high frequencies of forcing, but the experimental results indicate that the amplitude of the shear stress increases with increasing frequency (figure 21). Based on the above-mentioned discussion one may suggest that the variation of the amplitudes of $\langle u'^2 \rangle$, $\langle u'v' \rangle$ and $\langle \tau \rangle$ with frequency is not monotonic.

5. Conclusions

(i) Mean properties of the flow are not affected by pulsations in both laminar- and turbulent-flow regimes, provided the amplitude is not excessively high.

(ii) The oscillating part of the flow parameters can be represented by amplitude and phase at excitation frequency only. This representation becomes less accurate for turbulent quantities at higher amplitudes of forcing.

(iii) The radial distributions of amplitudes and phases of velocity oscillations are strongly dependent on the flow regime in the pipe (i.e. whether it is laminar or turbulent). The relatively low amplitudes of forcing used in the present work had little effect on the radial distributions of amplitudes and phase angles in the range of variables considered. The effect of Reynolds number on the phase distribution in the turbulent flow is substantially more significant.

(iv) A normalization procedure relating steady and oscillating components in turbulent flow was suggested; a fair agreement was found between the properly normalized time-averaged and time-dependent quantities for the entire range of frequencies considered.

(v) Slow adaptation of turbulence is responsible for some important features in the radial distributions of the turbulent quantities and their phase relations.

This work was supported in part by a grant from the Air Force Office of Scientific Research no. 77-3275.

REFERENCES

BROWN, F. T., MARGOLIS, D. L. & SHAH, R. P. 1969 Small-amplitude frequency behavior of fluid lines with turbulent flow. *Trans. ASME* D: *J. Basic Engng* **91**, 678–693.

CARO, C. G., PEDLEY, T. Y., SCHROTTER, R. C. & SEED, W. A. 1978 *The Mechanics of the Circulation*. Oxford University Press.

DENISON, E. B. 1970 Ph.D. Thesis, Purdue University, Lafayette, Ind.

DENISON, E. B., STEVENSON, W. H. & FOX, R. W. 1971 Pulsating laminar flow measurements with a directionally sensitive laser velocimeter. *AIChE J.* **17**, 781–787.

HUSSAIN, A. K. M. F. 1977 Mechanics of pulsatile flows in relevance to the cardiovascular systems. In *Cardiovascular Flow Dynamics and Measurements* (ed. N. H. C. Hwang & N. A. Normann). Baltimore: University Park Press.

HUSSAIN, A. K. M. F. & REYNOLDS, W. C. 1970 The Mechanics of an organized wave in turbulent shear flow. *J. Fluid Mech.* **41**, 241–258.

KIRMSE, R. E. 1979 Investigations of pulsating turbulent pipe flow. *Trans ASME* I: *J. Fluids Engng* **101**, 436–442.

LAUFER, J. 1954 *NACA Rep. No.* 1174.

LAUFER, J. & BADRI NARAYANAN, M. A. 1971 Mean period of the turbulent production mechanism in a boundary layer, *Phys. Fluids* **14**, 241–258.

OSTER, D. 1980 Ph.D. Thesis, Tel-Aviv University, Tel-Aviv.

OSTER, D. & WYGNANSKI, I. 1982 The forced mixing layer between parallel streams. *J. Fluid Mech.* **123**, 91–130.

NARASIMHA, R. & PRABHU, A. 1972 Equilibrium and relaxation in turbulent wakes. *J. Fluid Mech.* **54**, 1–17.

NEE, V. W. & KOVASZNAY, L. S. G. 1969 Simple phenomenological theory of turbulent shear flows. *Phys. Fluids* **12**, 473–484.

RAMAPRIAN, B. R. & TU, S.-W. 1980 An experimental study of oscillatory pipe flow at transitional Reynolds numbers. *J. Fluid Mech.* **100**, 513–544.

SCHLICHTING, H. 1975 *Boundary Layer Theory*. McGraw-Hill.

SEXL, T. 1930 Ueber den von E. G. Richardson entdeckten 'Annulareffekt', *Z. Phys.* **61**, 349–362.

SHEMER, L. 1981 Ph.D. Thesis, Tel-Aviv University, Tel-Aviv.

SHEMER, L. & KIT, E. 1984 An experimental investigation of the quasi-steady turbulent pulsating flow in a pipe. *Phys. Fluids* **27**, 72–76.

SHEMER, L. & WYGNANSKI, I. 1981 Pulsating flow in a pipe. In *Proc. 3rd Symp. on the Turbulent Shear Flows, Davis, Cal.*, 8.13–8.18.

TU, S.-W. & RAMAPRIAN, B. R. 1983 Fully developed periodic turbulent pipe flow in a tube. *J. Fluid Mech.* **137**, 31–58.

UCHIDA, S. 1956 Pulsating viscous flow superposed on the steady laminar motion. *Z. angew. Math. Phys.* **7**, 403–422.

WOMERSLEY, J. R. 1955 Method for the calculation of velocity rate of flow and viscous drag in arteries when the pressure gradient is known. *J. Physiol.* **127**, 553–572.

WYGNANSKI, I. J. & CHAMPAGNE, F. H. 1973 On transition in a pipe. Part I. The origin of puffs and slugs and the flow in a turbulent slug. *J. Fluid Mech.* **59**, 281–335.